This article has been accepted for publication in a future issue of this journal, but has not been fully edited. Content may change prior to final publication. Citation information: DOI 10.1109/ACCESS.2021.3124453, IEEE Access

IEEE Access
Multidisciplinary | Rapid Review | Open Access Journal

Date of publication xxxx 00, 0000, date of current version xxxx 00, 0000.

Digital Object Identifier 10.1109/ACCESS.2017.Doi Number

A New Vegetation Index in Short-Wave Infrared Region of Electromagnetic Spectrum

Yucel Cimtay[1], Busra Ozbay[2], Gökçe Nur Yilmaz[1], Eda Bozdemir[3]

[1]Computer Engineering Department, TED University, Ankara, Turkey

[2] Signal and Image Processing Group, HAVELSAN, Ankara, Turkey

[3] Department of Cell Systems and Anatomy, University of Texas Health Science Center at San Antonio, San Antonio, Texas, USA

Corresponding author: Yucel CIMTAY (e-mail: yucel.cimtay@tedu.edu.tr).

ABSTRACT Vegetation index algorithms based on radiance and/or reflectance data in the Visible Near Infrared (VNIR) band are created for multispectral and hyperspectral images to detect vegetation. By this way, vegetation and soil regions can be separated from each other. Furthermore, vegetation maturity and health can be observed and tracked. Besides VNIR band cameras, there are many cameras working in the Short Wavelength Infrared (SWIR) band. Therefore, the plant areas should also be detected in SWIR band images. For the purpose of the vegetation detection, a new vegetation index algorithm is created for SWIR hyperspectral images in this research. The proposed method's feasibility and precision is evaluated using SWIR band hyperspectral data collected at various locations and times during the year. Test results show that besides vegetation regions, soil and water regions in the SWIR band hyperspectral images can be detected successfully. On Hyperion hyperspectral data, 98.9% and 98.5% mean scores are achieved for recall and precision, respectively.

INDEX TERMS Vegetation index; Short wave infrared; Hyperspectral image; Precision Agriculture

I. INTRODUCTION

With the development of Hyperspectral imaging and processing technologies, precision agriculture applications have become favoured in recent years. Hyperspectral imaging and image processing methods are used in plant protection, detection of weeds, pests and diseases, and annual crop yield estimation [1, 2].

Detection of plant areas in the land cover by remote sensing has gained great importance in terms of precision agricultural practices. For this purpose, several vegetation index estimation algorithms have been developed in the literature, especially in Visible Near Infrared (VNIR) band multispectral and hyperspectral images. Some of these algorithms are Normalized Difference Vegetation Index (NDVI), Green Normalized Difference Vegetation Index (GNDVI), Enhanced Vegetation Index (EVI), Leaf Area Index (LAI), Soil Adjusted Vegetation Index (SAVI), and Modified Chlorophyll Absorption in Reflectance Index (MCARI) [3].

The study in [4] presents a vegetation index based on the universal pattern decomposition method and [5] proposes a colour region based vegetation segmentation and classification index.

Besides, detection of vegetation, the health of the plants are also crucial for the agricultural applications. In this context, several indexes are developed. In [6], authors developed a plant stress detector called Copper Stress Vegetation Index (CSVI), which is capable of measuring the plant stress due to copper ingredients.

When pixel-based indexes or classification methods [7] are not sufficient, for instance, in some crucial applications like narcotic, to detect the sub-pixel targets, hyperspectral unmixing techniques have been applied [8].

Besides the VNIR band cameras, Short Wavelength Infrared (SWIR) sensors can also be used for vegetation index applications. Considering this motivation, in this study, a new index algorithm is developed for the detection of the plant regions and estimation of the plant index in the hyperspectral images taken in the spectral range of SWIR 1000-2500 nm.

The rest of the paper is organized as follows. In Section II, the related work is discussed. Hyperspectral image data used in this study is introduced in Section III. Section IV presents the proposed method in detail. The results and discussions are mentioned in Section V. Section VI concludes the paper and mentions the future work.

This work is licensed under a Creative Commons Attribution-NonCommercial-NoDerivatives 4.0 License. For more information, see https://creativecommons.org/licenses/by-nc-nd/4.0/

This article has been accepted for publication in a future issue of this journal, but has not been fully edited. Content may change prior to final publication. Citation information: DOI 10.1109/ACCESS.2021.3124453, IEEE Access

II. RELATED WORK

The NDVI [9] is one of the most widely used and applied indices calculated from multispectral and/or hyperspectral data as a normalized ratio between the red and near infrared bands. Since the NDVI is frequently used to describe canopy growth or health, several studies have compared it to the Leaf Area Index (LAI) [10], which is formulated as the ratio between exact leaf area and its projection area to the ground.

One of the first vegetation indexes, Ratio Vegetation Index (RVI), is put forth by Jordan [11]. It is based on the concept that vegetation leaves absorb more light in the red spectrum region compared to the infrared region. The RVI is formulated in (1), as follows:

$$RVI = \frac{RED}{NIR} \tag{1}$$

where, NIR and RED are the reflectance values at near infrared and red bands, respectively. However, when the vegetation density is lower and since RVI is sensitive to atmospheric effects, Difference Vegetation Index (DVI), which is sensitive to changing soil backgrounds, can be modelled as in (2) [12]:

$$DVI = NIR - RED \tag{2}$$

Another vegetation index, Perpendicular Vegetation Index (PVI), which relies on the fact that high difference means high biomass, is produced in [12]. It is based on the relative reflectance between soil and vegetation captured at the red and NIR bands and can be calculated as in (3):

$$PVI = \sqrt{(R_{soil} - R_{veg})^2{}_{RED} - (R_{soil} - R_{veg})^2{}_{NIR}} \tag{3}$$

One of the most used vegetation indexes is the NDVI, which is computed as presented in (4) [13]. The NDVI is successful in handling both high and low dense vegetation. Since a normalization factor is used in the denominator in (4), the index values change between 0 and 1. The index values close to 1 indicates denser vegetation.

$$NDVI = \frac{NIR - RED}{NIR + RED} \tag{4}$$

Atmospheric effects are also considered by scientists for the index computation. The study in [14] proposes an index called, Atmospherically Resistant Vegetation Index (ARVI). The formulation of the ARVI is given in (5).

$$ARVI = \frac{NIR - (BLUE - RED)}{NIR + (BLUE - RED)} \tag{5}$$

The ARVI is successful in eliminating atmospheric aerosol.

Green Atmospherically Resistant Index (GARI) studied in [15] is more sensitive to chlorophyll concentrations and less sensitive to atmospheric effects than the NDVI. The formulation of the GARI is given in (6).

$$GARI = \frac{NIR - (GREEN - \rho(BLUE - RED))}{NIR - (GREEN - \rho(BLUE - RED))} \tag{6}$$

where, ρ is a weighting constant with respect to aerosol conditions.

Soil adjusted vegetation indexes are also studied widely in literature. One of these kinds of indexes is the SAVI which is proposed in [16]. This index suppresses the effects of the soil. This index gives very promising results in the areas with relatively sparse vegetation and visible soil. The formulation of the SAVI is given in (7).

$$SAVI = \frac{1.5 * (NIR - RED)}{NIR + RED + 0.5} \tag{7}$$

The study in [17] proposes the optimized SAVI by using a standard background adjustment factor. Another soil adjusted index is Modified Soil Adjusted Index (MSAVI2), which is put forth in [18] and formulated as in (8).

$$MSAVI2 = \frac{2 * NIR + 1 - \sqrt{(2 * NIR + 1)^2 - 8(NIR - RED)}}{2} \tag{8}$$

The MSAVI2, as the simpler version of the SAVI which is proposed in [16], minimizes the soil noise and improves the dynamic range of the signal reflected by the vegetation.

There are also vegetation indexes based on Chlorophyll Absorption Ratio such as Modified Chlorophyll Absorption Ratio Index Improved (MCARI2) [19]. The MCARI2 is an accurate predictor of the green leaf area index. The calculation of the MCARI2 is given in (9)

$$MCARI2 = \frac{1.5 * [2.5(R_{800} - R_{670}) - 1.3(R_{800} - R_{670})]}{\sqrt{(2 * R_{800} + 1)^2 - (6 * R_{800} - 5 * \sqrt{R_{670}}) - 0.5}} \tag{9}$$

Here, R_{800} and R_{670} are the reflectance values at 800nm and 670nm wavelengths, respectively.

Besides the vegetation indexes studied in the VNIR band, there are several studies, which use bands from both the VNIR and SWIR bands [20]. The study in [21] uses a vegetation index, which relies on the normalized ratio of

This work is licensed under a Creative Commons Attribution-NonCommercial-NoDerivatives 4.0 License. For more information, see https://creativecommons.org/licenses/by-nc-nd/4.0/

This article has been accepted for publication in a future issue of this journal, but has not been fully edited. Content may change prior to final publication. Citation information: DOI 10.1109/ACCESS.2021.3124453, IEEE Access

bands 8 and 11 from Sentinel-2. Band-8 corresponds to 865nm and band-11 corresponds to 1610nm. Therefore, band-8 is from the VNIR band and band-11 is from the SWIR band. Similarly, the study in [22] creates a vegetation index called Normalized Burn Ratio Index (NBR). The NBR uses band-9 and band-12 from Sentinel-2 imagery. These bands correspond to 940nm and 1290nm respectively. In [23], another vegetation index called Global Vegetation Moisture Index (GVMI) is created which uses the same bands as in [22] but with some offset added to radiance values of both bands. In [24], again the same bands are used. However, in this study, the vegetation index relies on a simple ratio of the two bands. Another study which uses bands both from the VNIR and SWIR regions is [25]. In this study, the RED band used in any vegetation indexes in the VNIR region is replaced with a band from the SWIR region which corresponds to the 1628-1652 nm spectral interval. This study concludes that replacing the RED band with the SWIR band reduces the sensitivity of vegetation indexes to soil background.

NDMI [26] (Normalized Difference Moisture Index) is another index which is used for detection of water. It is developed on Landsat-7 and Landsat-8 imagery. In this index both the VNIR and SWIR bands are used. For the Landsat-7 and Landsat-8; band-4 and band-5, band-5 and band-6 are used, respectively. One of the bands corresponds to the VNIR region and the other one to the SWIR region. Another index which is sensitive to canopy water content is NDWI (Normalized Difference Water Index) which is presented in [27]. This index uses the bands corresponding to 857 nm and 1241 nm wavelengths, respectively. MNDWI (Modified Normalized Difference Water Index) which is created by Xu.H [28] uses a green band and one band from the SWIR region. A recent study conducted in [29] presents a time-series comparison of vegetation indexes. Figure 1 shows the correlation between vegetation indices. The indices created using spectral bands from VNIR and SWIR regions exhibit a high correlation, which is between 0.94 and 1. The indices in the VNIR range had more fluctuation, with r-values ranging between 0 and 0.99.

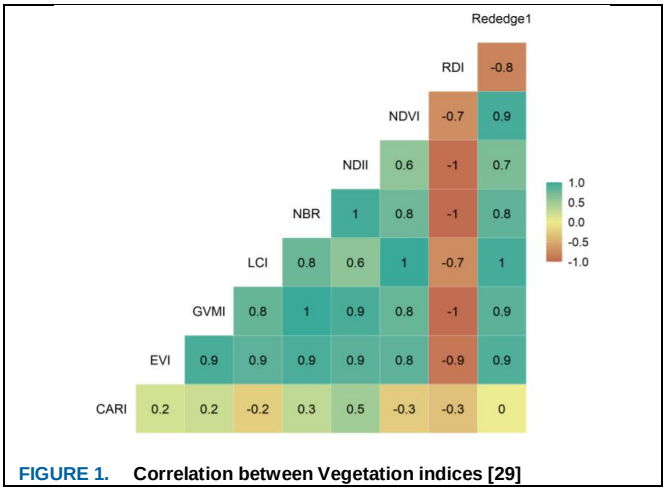


FIGURE 1. Correlation between Vegetation indices [29]

Another study, which is conducted in [30], discusses and compares vegetation indices. Based on green leaf estimation error, it reports that the best three vegetation indices are EVI, $(CI)_{red\text{-}edge.}$ and MERIS Terrestrial Chlorophyll Index (MTCI).

The vegetation indexes in the VNIR bands are useful, however they do not work when one has only the SWIR bands. The hybrid indexes which use bands from both the VNIR and SWIR regions need special cameras and/or satellites which carry both the VNIR and SWIR sensors. Another problem is the spectral similarity between soil and water or water and soil in the SWIR band. There are many multispectral and/or hyperspectral cameras which are working in the SWIR region. Therefore, scientists need to detect the vegetation areas and estimate the vegetation index by only using the SWIR band image data.

In the light of these discussions, considering that there is lack of SWIR band-based vegetation indexes in the literature, a vegetation index called Short Wave Normalized Vegetation Index (SWNWI), which can detect the vegetation, estimate the vegetation index and solve the problem of misdetections pointed to soil-water or plant-water, is proposed in this study.

The contributions of the proposed method are the following:

- Proposed index uses only the SWIR region bands and does not need any bands from the VNIR or any other region.

- Previous vegetation indexes can only detect vegetation and soil or only water content of vegetation. However, the proposed index can classify land cover as water, soil, vegetation and estimate the vegetation index in the SWIR band images.

This work is licensed under a Creative Commons Attribution-NonCommercial-NoDerivatives 4.0 License. For more information, see https://creativecommons.org/licenses/by-nc-nd/4.0/

This article has been accepted for publication in a future issue of this journal, but has not been fully edited. Content may change prior to final publication. Citation information: DOI 10.1109/ACCESS.2021.3124453, IEEE Access

III. HYPERSPECTRAL IMAGE DATA

A. HySpex Data

Hyperspectral images belonging to HySpex Camera have 5.45 nm spectral resolution and 288 spectral bands in [1000-2500] nm spectral range. The images are captured by using HySpex SWIR 384 Linear Array Hyperspectral Camera [31] which is shown in Figure 2. This camera is mounted on a plane, which flies over and covers the target area. The spatial resolution is adjusted as (2.19 x 2.19) m2.



FIGURE 2. HySpex SWIR 384 Linear Array Hyperspectral Camera [29]

The vegetation index algorithm proposed in this study is developed on the SWIR band images. To evaluate the performance of the proposed method, the visual comparison and error estimation are conducted with the mostly used and successful vegetation index NDVI that is estimated from the VNIR images. To capture the VNIR band images, HySpex VNIR-1800 Linear Array Hyperspectral Camera is used [32]. The VNIR band images have 3.2 nm spectral resolution with 182 spectral bands in the [400-1000] nm spectrum. The spatial resolution is adjusted as (60x60) cm2.

When collecting image data, both the SWIR and VNIR cameras are mounted on the same platform. Therefore, at the time of the flight, the data from both cameras are recorded simultaneously. To overcome the issue of having different spatial resolutions for the VNIR and SWIR cameras, the SWIR image is registered on the VNIR image by interpolating the SWIR data. As a result, we obtain the same number of pixels in both the SWIR and VNIR images.

The images used in this work are radiance images and geometric correction is applied on the raw image data. To make an accurate geo-correction, we put GCP (Ground Control Points) on the region by using a GPS device. Figure 3 shows the Google Earth image of the target area in Harran plain and the GCP points (yellow pointers) put on the region.



FIGURE 3. Harran Region in Google Earth and GCP points

Hyperspectral VNIR and SWIR band images used in this study are captured from the Harran plain region where wheat, corn, and cotton planting are widespread. Besides, the images also include water channels and soil areas. A regular RGB camera image taken from ground is shown in Figure 4. At the time of the image taken, cotton is newly planted and very young. However, in August, corn becomes taller, the leaves get wider.



FIGURE 4. A cotton field from Harran Plain, Turkey, captured in April 2018

B. Hyperion Data

Hyperion is a push-broom hyperspectral instrument [33] on board the EO-1 satellite, which is shown in Figure 5. It gathers 220 distinct spectral channels with a 10-nm bandwidth ranging from 357 nm to 2576 nm. The spatial resolution is 30x30 m2 for all bands. Since Hyperion includes both the VNIR and SWIR bands, it is convenient to estimate the NDVI from the same image, besides SWNVI.

This work is licensed under a Creative Commons Attribution-NonCommercial-NoDerivatives 4.0 License. For more information, see https://creativecommons.org/licenses/by-nc-nd/4.0/

This article has been accepted for publication in a future issue of this journal, but has not been fully edited. Content may change prior to final publication. Citation information: DOI 10.1109/ACCESS.2021.3124453, IEEE Access

The Hyperion images are already geometrically corrected; therefore, a geometric correction is not needed.

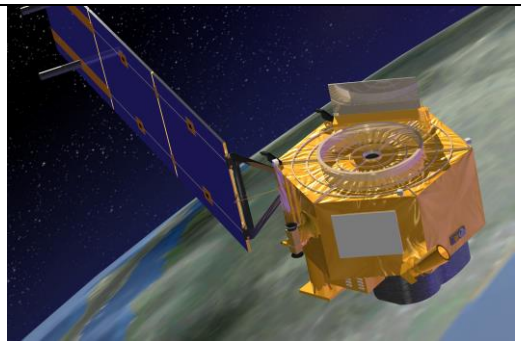


FIGURE 5. EO-1 Satellite [33]

Spectra extracted from water, plant and soil regions are shown in Figure 6 along the VNIR and SWIR bands for Hyperion image. In the SWIR band region, the spectra exhibit similar patterns in terms of the local maximum points; nonetheless, they are different from each other spectrally.

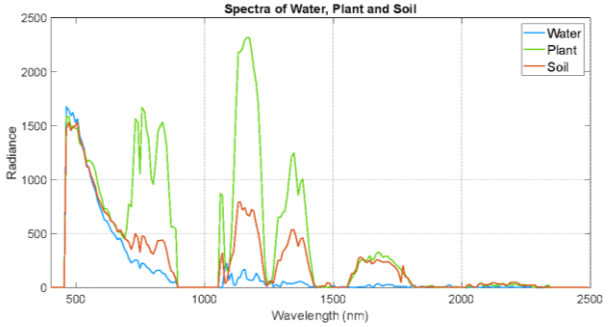


FIGURE 6. Hyperion Image, water, plant, and soil spectra

IV. PROPOSED METHOD

We develop the proposed index algorithm on the HySpex hyperspectral imagery data and apply it on the Hyperion hyperspectral imagery as well. In figure 7, an example of a false coloured SWIR image and the spectra extracted from the regions: plant, soil and water are shown for the HySpex camera imagery. The pink, green and dark regions show vegetation, soil, and water channels, respectively. Figure 7-b is handled by using ENVI program [34].

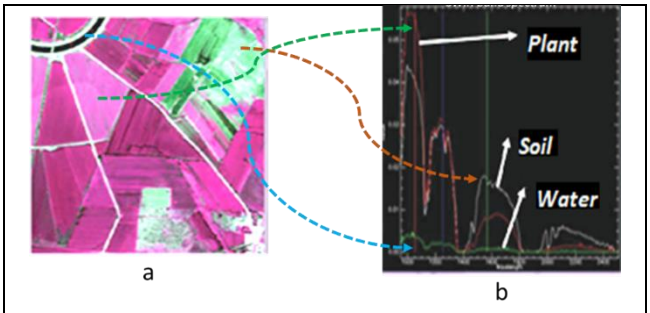


FIGURE 7. a-False coloured HySpex SWIR band image b-Plant, soil, and water spectra.

The gradient of the spectra of plant, soil and water extracted from the SWIR image are examined and it is observed that the spectra behave in a way to create four different local maximum regions in the band interval [1000, 2500] nm. Local maximum or minimum values are the points where the derivative of the function approaches zero. These kinds of points are widely used for data analysis. In this study, rather than single points, specific regions where the derivative approaches zero are considered.

In this study, atmospheric blocking bands around 1100 nm, 1250 nm, 1400 nm and 1950 nm are excluded, so that they are not used in this study. Specific wavelength intervals are determined around the local maximum values. These are [1000-1060] nm, [1535-1650] nm and [2100-2200] nm, respectively, for HySpex data. By calculating the mean radiance along these intervals, 3 different mean radiance values R_1, R_2 and R_3 are handled. The decaying characteristics of the spectra along these intervals are similar but not the same for plant, soil, and water. For the calculation of R_1, all bands fall in the interval [1000-1060] is read from the image data. Then, the mean value is calculated by using (10) where $B_{[1000-1060]}$ is the sequence of all bands that fall inside [1000,1060] nm and N_1 is the number of bands.

$$R_1 = \frac{\sum B_{[1000-1060]}}{N_1} \tag{10}$$

Similarly, R_2 and R_3 are calculated by using (11) and (12), where N_2 and N_3 are the number of bands inside the related wavelengths.

$$R_2 = \frac{\sum B_{[1535-1650]}}{N_2} \tag{11}$$

$$R_3 = \frac{\sum B_{[2100-2200]}}{N_3} \tag{12}$$

This work is licensed under a Creative Commons Attribution-NonCommercial-NoDerivatives 4.0 License. For more information, see https://creativecommons.org/licenses/by-nc-nd/4.0/

This article has been accepted for publication in a future issue of this journal, but has not been fully edited. Content may change prior to final publication. Citation information: DOI 10.1109/ACCESS.2021.3124453, IEEE Access

Following the estimation of mean radiance values, the first step is calculating the Normalized Difference Index (NDI) by using the mean radiances. The calculation of the NDI between any two bands are given in (13), where R_a and R_b are radiance/reflectance values of any bands a and b.

$$NDI = \frac{R_a - R_b}{R_a + R_b} \tag{13}$$

By getting use of the radiance level differences between soil, plant and water spectra along local maximum regions, the reason for NDI estimation is to separate the water, soil and vegetation regions. NDI between R_1 and R_2, R_1 and R_3, R_2 *and* R_3 is estimated. Even though plant and soil separation can be achieved successfully in the results, it has been observed that there is large similarity between the NDIs of water and soil regions. This led us to develop a two-stage index algorithm for SWIR band imagery. In the first step, a water index is created from the mean radiances. As R_1, R_2 and R_3 are the mean radiance values between [1000-1060] nm, [1535-1650] nm and [2100-2200] nm wavelength intervals respectively, Water index (WI) is formed by using (14).

$$WI = \frac{R_1 - R_2}{R_1 + c_1 * R_1 - c_2 * R_3 + L} * G \tag{14}$$

Since, aerosol is effective around R_2 band like between [1630, 1650] nm, R_3 band is used to correct the atmospheric effects like aerosol on R_2 band. c_1 and c_2 are the coefficients of aerosol resistance terms. L is the background adjustment term, which covers nonlinearity between R_1 and R_2 bands and G is the gain factor. Optimal coefficients, gain and background adjustment terms are determined empirically by conducting independent trials. The ideal condition is that water regions can be separated from plant and/or soil regions almost perfectly. Finally, the coefficients, background resistance term and gain are adopted as $c_1 = 6$, $c_2 = 7.5$, L=1 and $G = 2.5$.

In this study, as the second step, another index which is called Plant Index (PI) are created by using (15). New coefficients, atmospheric resistance term and gain are adopted in a similar manner as it is done for water index. The equation is similar to the one used in [35], however the coefficients are adopted according to the bands in the SWIR region, since we are using bands only from the SWIR region. (PI) has the capability of separating plant and soil. WI and PI are fused to separate soil, water, and plant regions. The meaning of fusion in this concept is first applying the Water Index on the image and excluding the detected water regions from the whole set. Secondly applying Plant Index on the resulting map from the first step. Finally fusing the result maps estimated from WI and PI to handle the final classification map (water, soil and plant).

$$PI = \frac{R_1 - R_2}{4 * R_1 + R_2 - 2 * R_3} * 2 \tag{15}$$

In (14) and (15) the base index equations are scaled by some coefficients to attenuate the atmospheric effects. The optimal coefficient values are determined empirically by conducting independent trials. The index values handled from WI are passed through a thresholding process. In this way, water regions are separated from vegetation and soil.

Plant and soil cannot be separated by WI, therefore they are separated from each other by applying PI after WI by excluding the water regions detected in the first step. The proposed Short Wave Normalized Vegetation Index (SWNVI) is the fusion of PI andWI. SWNVI is capable of separating plant, soil, and water regions from each other and estimating the vegetation index map which gives information about vegetation maturity and health.

In the proposed method, high PI values indicate the regions with dense green vegetation, whereas the low values indicate the regions where the cultivation is not carried out properly, or the regions where the plant is unhealthy due to various reasons such as drought, disease, and pests.

V. RESULTS AND DISCUSSIONS

Proposed approach is tested on two different SWIR image datasets: HySpex and Hyperion Imagery. Although the proposed index can separate soil, water, and plant regions successfully, for a comparison with the VNIR band vegetation index, the NDVI is also estimated on the VNIR images of the same regions. Figure 7-9 contain the result maps showing the SWIR, VNIR, NDVI and Plant Index (PI) for each hyperspectral imagery handled from HySpex.

In Figure 8-10, (a) is VNIR images, (b) shows the NDVI result map of the image in (a). The map in (d) shows Plant Index (PI) result of the SWIR image shown in (c). In the maps (b) and (d), warm colours (yellow and orange) indicate the greenest areas, while the cold colours (blue) indicate the soil and water areas. The pink regions in SWIR images represent the plant areas. Note that VNIR and SWIR images shown in Figure 8-10 are handled by applying radiometric and geometric correction on the raw hyperspectral images.

This work is licensed under a Creative Commons Attribution-NonCommercial-NoDerivatives 4.0 License. For more information, see https://creativecommons.org/licenses/by-nc-nd/4.0/

This article has been accepted for publication in a future issue of this journal, but has not been fully edited. Content may change prior to final publication. Citation information: DOI 10.1109/ACCESS.2021.3124453, IEEE Access

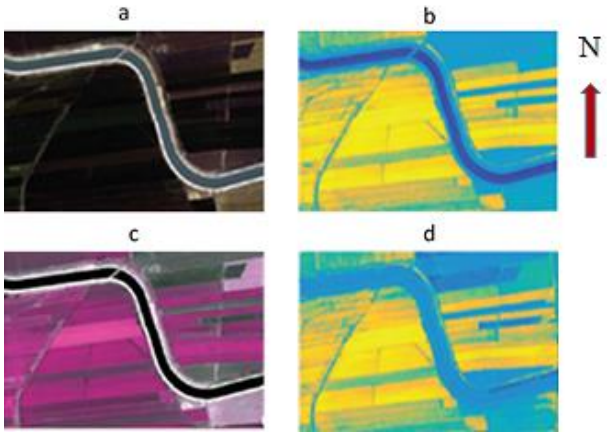


FIGURE 8. Images and Index Maps-1. a-VNIR band image b-NDVI Map c-SWIR band image d-SWNVI Map

In Figure 8 and Figure 9, there are green vegetation, soil, and water regions. The water channel is full of water. It can be observed from the results that the success of the proposed method is on par with the NDVI results. Here, the vegetation regions are compared, the water channel is not compared. As it is seen from the figures, water and soil regions are the tones of blue. Therefore, a traditional vegetation index in the SWIR region cannot separate the water and soil areas due to their similar spectral properties. This problem creates the core of our study. This is the reason for developing a two-stage SWIR index as introduced in the proposed method section.

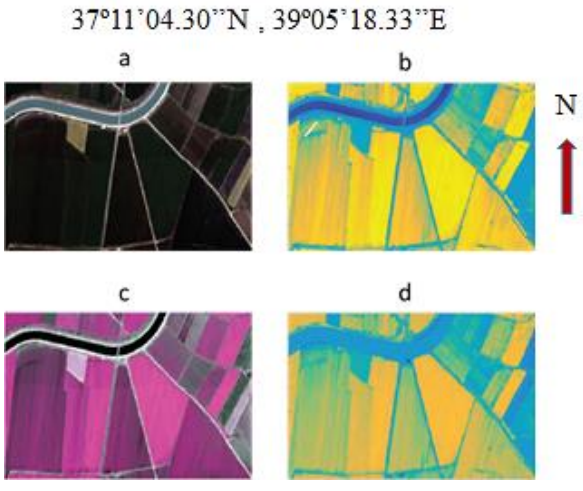


FIGURE 9. Images and Index Maps-2. a-VNIR band image b-NDVI Map c-SWIR band image d-SWNVI Map

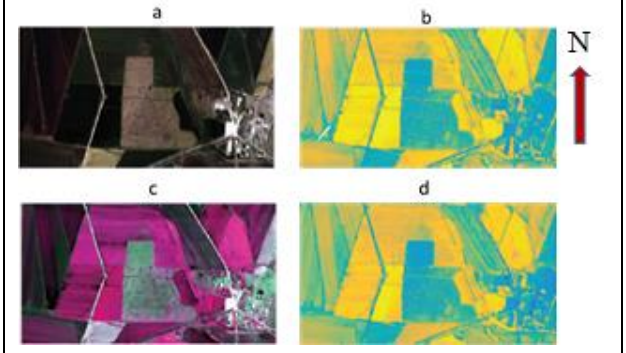


FIGURE 10. Images and Index Maps-3. a-VNIR band image b-NDVI Map c-SWIR band image d-SWNVI Map

For the comparison of vegetation index values, we first applied WI to exclude the water regions. After applying the PI and NDVI, we normalize NDVI and SWNVI index values to [0, 1] interval and calculate Mean Square Error (MSE) between the NDVI and SWNVI index maps by using (16) where N is the number of pixels in resulted maps and i represents pixel indices in the resulted vegetation maps created by the NDVI and SWNVI.

$$MSE = \frac{1}{N}\sum_{i=1}^{N}(NDVI_i - SWNVI_i)^2 \qquad (16)$$

The MSEs are presented in Table-I for three different SWIR images shown in Figure 8-10. MSEs Values are very low which shows that the proposed vegetation index is totally on par with NDVI.

TABLE I
MSE BETWEEN NDVI AND SWNVI FOR THREE DIFFERENT SCENES FROM HARRAN, TURKEY

Error Metric	Index Map-1	Index Map-2	Index Map-3
MSE	0.0009	0.0003	0.0001

We have also tested the proposed index algorithm on Hyperion imagery. The bands in the SWIR region (1000-2500nm) are used. Each test image covers roughly 900 km^2, which is required and sufficient to prove the reliability of the proposed method. The area of the Hyperion images is calculated by using QGIS Geographic Information Software Tool [36]. Figure 11-a shows the real colour image from Galapagos Island. This image includes water, soil and plant regions as shown in Figure 11-b which is the ground truth image. Plant Index (PI) is

This work is licensed under a Creative Commons Attribution-NonCommercial-NoDerivatives 4.0 License. For more information, see https://creativecommons.org/licenses/by-nc-nd/4.0/

This article has been accepted for publication in a future issue of this journal, but has not been fully edited. Content may change prior to final publication. Citation information: DOI 10.1109/ACCESS.2021.3124453, IEEE Access

applied to that hyperspectral image and the resulting index map is passed through a thresholding process. The threshold value is chosen as 0.7. The resulting index image is shown in Figure 11-c. It can be observed that the plant regions are detected well. Moreover, with respect to the image shown in (a), plant and soil can be separated accurately. However, it is obvious that water regions are misclassified as plants. Note that the misclassification can change according to the scene and type of SWIR sensor. It can be water-soil (as in Hyspex) or water-plant (as in Hyperion) misdetections.

To overcome this problem, we apply the water index which is given in (14). By this way, we can detect and eliminate the water regions first. The resulting water index map is shown in Figure 11-e. By this way, water areas are detected. Then the result maps of water index and plant index are fused with some morphological image processing techniques applied, the resulting image is shown in Figure 11-f. The brown areas are soil regions. The blue and green areas are water and plant regions, respectively. This result substantially matches the ground truth image shown in 11-b.

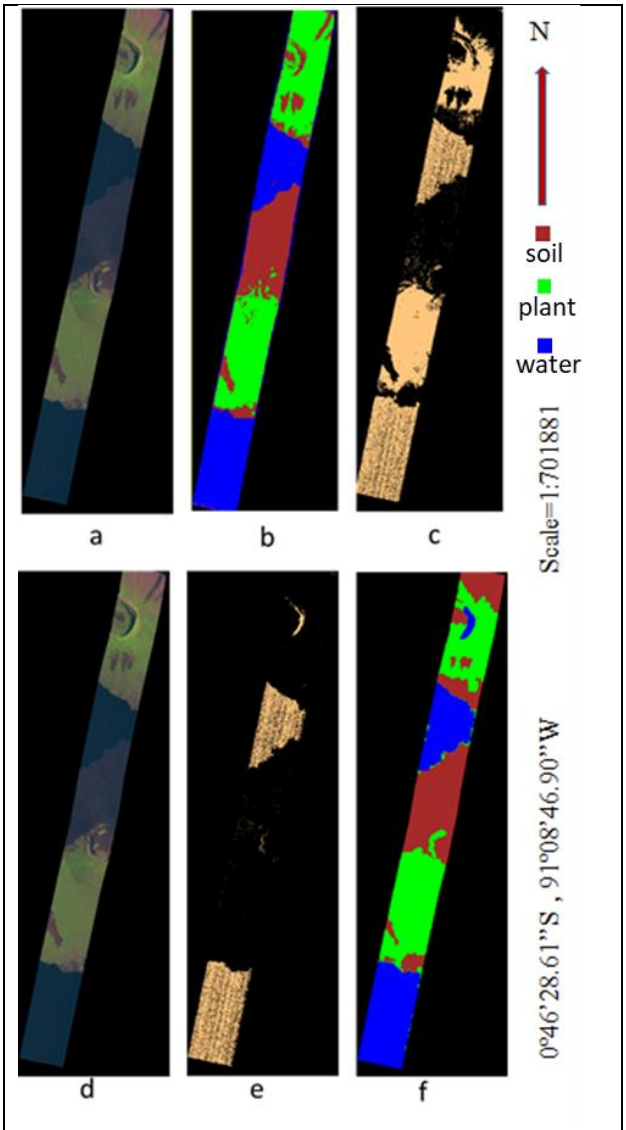


FIGURE 11. **Hyperion Image from Galapagos island. a- RGB bands b-Ground truth c-Plant areas detected by plant index d-RGB bands e-Water index map f-Classification of soil, plant, and water**

Figure 12 shows another Hyperion image, which is captured from Algeria. This area includes only soil. Therefore, the proposed index is expected not to detect any plant and/or water regions. Thus, as Figure 12-d shows the resulting map, it has only brown areas, which represent the soil. This is a promising result. Figure 12-b is the water index map and 12-c is the plant index map. Since there is no water and plant areas, the resulting index maps are black which means “no target point”.

This work is licensed under a Creative Commons Attribution-NonCommercial-NoDerivatives 4.0 License. For more information, see https://creativecommons.org/licenses/by-nc-nd/4.0/

This article has been accepted for publication in a future issue of this journal, but has not been fully edited. Content may change prior to final publication. Citation information: DOI 10.1109/ACCESS.2021.3124453, IEEE Access

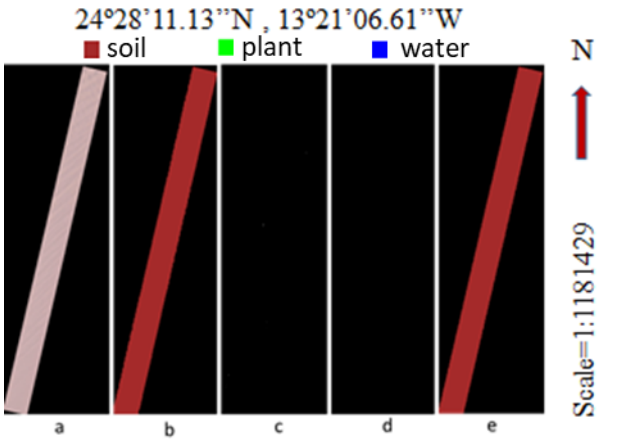


FIGURE 12. **Hyperion Image from Algeria. a- RGB bands b-Ground-truth c-Plant areas detected by plant index d-Water index map e-Classification of soil, plant, and water (result of SWNVI)**

Figure 13 shows another Hyperion image, which is captured from Australia. This image includes soil and plant areas. In Figure 13-b, except '6' image points (pixels), no water regions are detected as expected. These 6 points are obviously false detections. 13-c shows the plant index map and 13-d shows the classification of land cover as soil and plant. It does not include any water regions as expected.

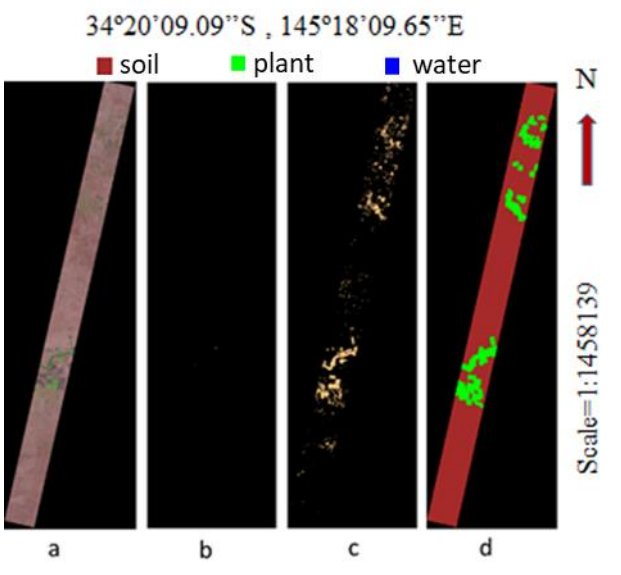


FIGURE 13. **Hyperion Image from Australia. a- RGB bands b-Water areas detected by water index c-Plant index map d-Classification of soil, plant, and water**

The proposed index method achieves accurate results on another Hyperion image, which is captured from Santa Monica (California). Figure 14 shows the results handled.

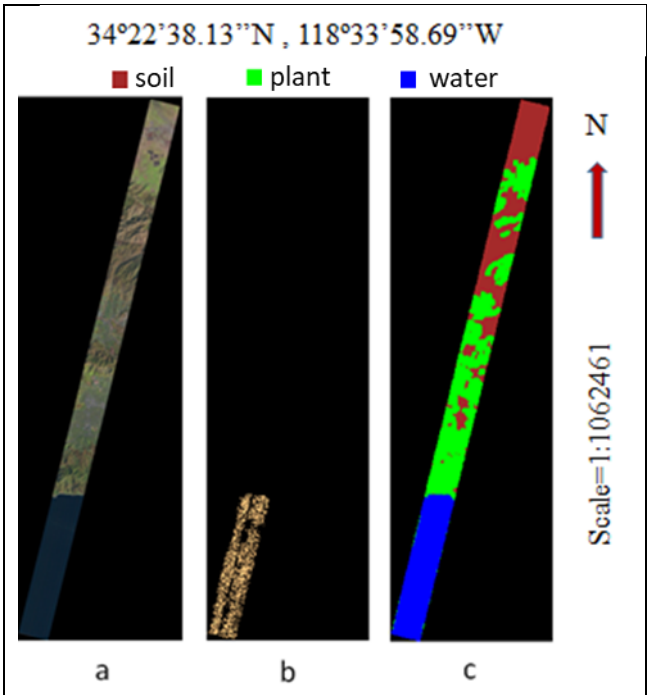


FIGURE 14. **Hyperion Image from Santa Monica (California). a- RGB bands (ground truth) b-Water areas detected by water index c-Classification of soil, plant, and water**

Table II-V shows the recall and precision scores for the hyperspectral images in Figure 11-14. Note that recall and precision scores are calculated between ground truth (soil, plant, water) and classification output image of the SWNVI. Table VI shows the mean recall and precision scores for each image and are calculated by using all recall and precision scores for each of soil, plant and water.

TABLE II
RECALL AND PRECISION SCORES FOR IMAGES IN FIGURE 11.

Galapagos	Recall (%)	Precision (%)
Water	99.7	97.2
Soil	99.1	97.3
Plant	96.4	98.5

TABLE III
RECALL AND PRECISION SCORES FOR IMAGES IN FIGURE 12.

Algeria	Recall (%)	Precision (%)
Water	-	-
Soil	100	100
Plant	-	-

This work is licensed under a Creative Commons Attribution-NonCommercial-NoDerivatives 4.0 License. For more information, see https://creativecommons.org/licenses/by-nc-nd/4.0/

This article has been accepted for publication in a future issue of this journal, but has not been fully edited. Content may change prior to final publication. Citation information: DOI 10.1109/ACCESS.2021.3124453, IEEE Access

TABLE IV
RECALL AND PRECISION SCORES FOR IMAGES IN FIGURE 13.

Australia	Recall (%)	Precision (%)
Water	-	-
Soil	97.3	99.1
Plant	99.2	98.2

TABLE V
RECALL AND PRECISION SCORES FOR IMAGES IN FIGURE 14.

Santa Monica	Recall (%)	Precision (%)
Water	99.8	99.4
Soil	98.7	97.6
Plant	98.9	96.5

TABLE VI
AVERAGE RECALL AND PRECISION SCORES FOR IMAGES IN FIGURE 11-14.

Image	Recall (%)	Precision (%)
Galapagos	98.4	97.6
Algeria	100	100
Australia	98.2	98.6
Santa Monica	99.1	97.8
Average	98.9	98.5

Figure 15 shows the comparison of the NDVI and SWNVI index maps. As it is observed from the figure, they are very similar to each other. The index values are normalized between '0' and '1' and MSE between two index maps is calculated. Table VII shows the MSE scores for each Hyperion image captured from Galapagos and Australia. It does not include Algeria since we do not have any plant regions. As it is seen from the table, the MSE scores are very low, which means high correlation and similarity. These results show that the SWNVI can handle vegetation indexes as successfully as the NDVI. This means that the SWIR cameras can also be used for classification of land cover as soil, vegetation, and water. Since the NDVI is a measure of plant maturity (young plants with low NDVI and mature ones with higher NDVI [29]) and the PI of SWNVI exhibits high correlation with NDVI regarding vegetation index estimation, SWNVI can also be used as a measure of the maturity and/or health of vegetation. This is due to the high correlation between SWNVI and NDVI as the MSE for vegetation index estimation is very little. This is very important for farmers in terms of early detection of diseases and precision agriculture applications.

TABLE VII
MSE BETWEEN NDVI AND SWNVI HANDLED FROM HYPERION IMAGES

Error Metric	Galapagos	Australia
MSE	0.0009	0.0003

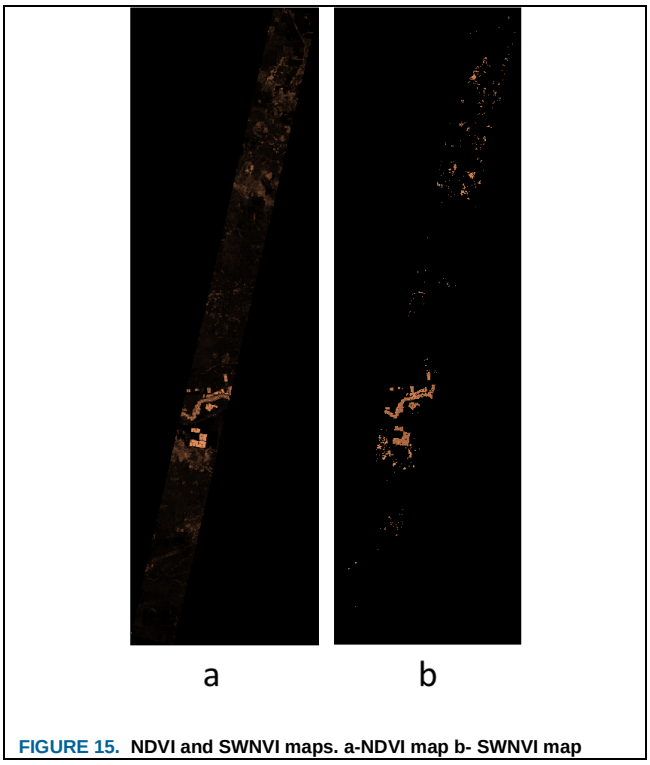


FIGURE 15. NDVI and SWNVI maps. a-NDVI map b- SWNVI map

In this study, the water index map is compared to the well-known canopy water index NDWI (Normalized Difference Water Index) [37, 38]. The formula of NDWI is given in (17).

$$NDWI = \frac{(R_{857} - R_{1241})}{(R_{857} + R_{1241})} \quad (17)$$

Figure 16 and 17 show the visual results for Galapagos and Santa Monica. The NDWI has not only the capability of estimating water content of the plant canopy but also the water regions. Note that the NDWI uses both spectral bands from the VNIR and SWIR region and our water index uses only bands from the SWIR region. It can be observed that the proposed water index can handle accurate results as NDWI

This work is licensed under a Creative Commons Attribution-NonCommercial-NoDerivatives 4.0 License. For more information, see https://creativecommons.org/licenses/by-nc-nd/4.0/

This article has been accepted for publication in a future issue of this journal, but has not been fully edited. Content may change prior to final publication. Citation information: DOI 10.1109/ACCESS.2021.3124453, IEEE Access

does. This shows the accuracy of the proposed method although it uses bands from only the SWIR region.

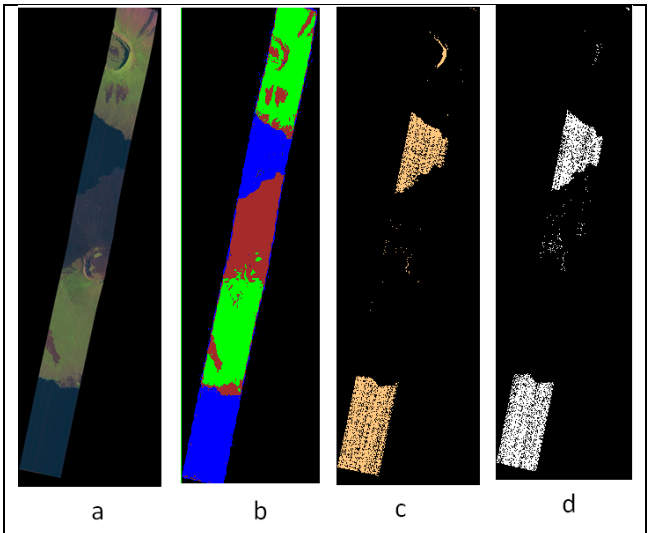


FIGURE 16. Hyperion Image from Galapagos island. a- RGB bands b-ground truth c-Proposed water index map d-Result map of NDWI

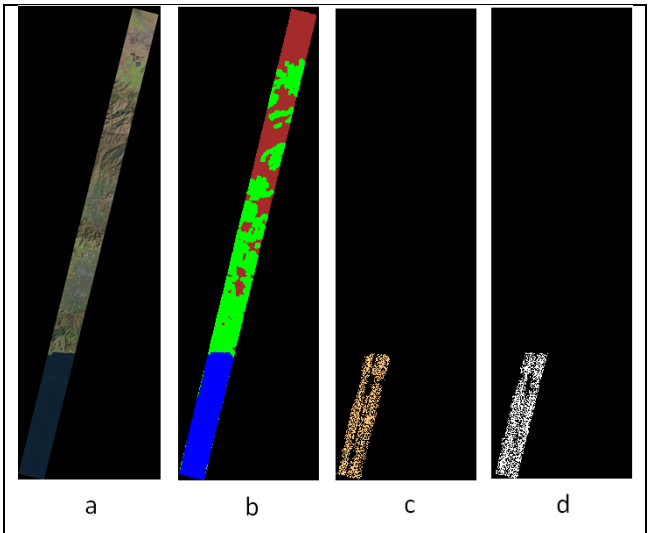


FIGURE 17. Hyperion Image from Santa Monica (California).a- RGB bands b-ground truth c-Proposed water index map d-Result map of NDWI

Table VIII and IX present the recall and precision score benchmark for the proposed water index and NDWI. As it can be observed from the tables, the proposed water index is as successful as NDWI. This shows the proposed water index (which is a part of the SWNVI) can successfully cover the water regions in hyperspectral images.

TABLE VIII
RECALL AND PRECISION SCORES FOR IMAGES IN FIGURE 16.

Galapagos	Recall (%)	Precision (%)
Proposed Water index	99.7	97.2
NDWI [38]	99.5	97.7

TABLE IX
RECALL AND PRECISION SCORES FOR IMAGES IN FIGURE 17.

Santa Monica	Recall (%)	Precision (%)
Proposed Water index	99.8	99.7
NDWI [38]	99.1	99.4

VI. CONCLUSIONS AND FUTURE WORK

This study is very important due to the fact that it can estimate vegetation index and classify soil, water and plant in the SWIR band images. This is because the vegetation index and/or water index methods conducted until now use bands from either the VNIR region or the VNIR and SWIR regions together whereas the proposed method uses bands from only the SWIR region. This is a good contribution to the literature because there are many applications, which use only hyperspectral cameras working in the SWIR region. However, when they want to implement precision agriculture projects, since they do not have the hyperspectral data in the VNIR region, they cannot estimate the vegetation index or classify the land cover area accurately. This is the main reason for proposing this study. Since, there are many applications, which need the SWIR band data, this study will enable those kinds of project holders to use SWIR band cameras also for agricultural applications without spending for another VNIR band camera and/or wide-band cameras. This will bring convenience and independence to them.

This study proposes a new index algorithm for detecting vegetation on land cover in the hyperspectral SWIR images. Since either water and soil or water, and plant cannot be separated from water SWIR bands easily, the proposed method has been developed in two-stages.

In the first step, a water index, which is given by (14), has been created. By this way, water regions in the imagery have been detected and separated. In the second step, plant and soil have been separated from each other by using a formulated plant index.

This work is licensed under a Creative Commons Attribution-NonCommercial-NoDerivatives 4.0 License. For more information, see https://creativecommons.org/licenses/by-nc-nd/4.0/

This article has been accepted for publication in a future issue of this journal, but has not been fully edited. Content may change prior to final publication. Citation information: DOI 10.1109/ACCESS.2021.3124453, IEEE Access

The classification performance of the proposed method, recall and precision scores have presented promising results which means most of the target points can be detected successfully and false detections are very little.

The vegetation index estimation performance of the proposed method has been compared to the NDVI maps, which have been estimated from the VNIR band images. Results have shown that the proposed index algorithm can achieve very accurate results compared with the NDVI map. Furthermore, the water index estimation performance of the proposed method has been compared with the NDWI and very promising results have been observed.

It can be clearly stated that our proposed method can separate soil, vegetation, and water from each other successfully. It can also give information about the health and maturity of vegetation since the NDVI has been used for measuring these kinds of indications. Since the theory and mathematics are very easy to implement, the proposed index algorithm can also be embedded and used in real-time agricultural applications in the future.

ACKNOWLEDGMENTS

The authors wish to express their appreciation to HAVELSAN A.S, for letting them use the hyperspectral image data; NASA and USGS for sharing Hyperion data with the public.

REFERENCES

[1] Zongmei Gao, Lav R. Khot, Rayapati A. Naidu, Qin Zhang, Early detection of grapevine leafroll disease in a red-berried wine grape cultivar using hyperspectral imaging, Computers and Electronics in Agriculture, Volume 179, 2020.

[2] Lin Yuan, Peng Yan, Wenyan Han, Yanbo Huang, Bin Wang, Jingcheng Zhang, Haibo Zhang, Zhiyan Bao, Detection of anthracnose in tea plants based on hyperspectral imaging, Computers and Electronics in Agriculture, Volume 167, 2019.

[3] Li, Chenzong, Xue, Jinru, Su, Baofeng, Significant Remote Sensing Vegetation Indices: A Review of Developments and Applications, 1353691, 2017

[4] Lifu Zhang, S. Furumi, K. Muramatsu, N. Fujiwara, M. Daigo & Liangpei Zhang (2007) A new vegetation index based on the universal pattern decomposition method, International Journal of Remote Sensing, 28:1, 107-124, DOI: 10.1080/01431160600857402

[5] Lee, MK., Golzarian, M.R. & Kim, I. A new color index for vegetation segmentation and classification. Precision Agric 22, 179–204 (2021). https://doi.org/10.1007/s11119-020-09735-1

[6] Chengye Zhang, Huazhong Ren, Qiming Qin & Okan K Ersoy (2017) A new narrow band vegetation index for characterizing the degree of vegetation stress due to copper: the copper stress vegetation index (CSVI), Remote Sensing Letters, 8:6, 576-585, DOI: 10.1080/2150704X.2017.1306135

[7] I. Karakaya and Y. Çimtay, "The effect of bant selection to success of artificial neural network in hyperspectral classification," 2017 25th Signal Processing and Communications Applications Conference (SIU), 2017, pp. 1-4, doi: 10.1109/SIU.2017.7960553.

[8] Yücel Çimtay, Hakkı Gökhan İlk, A novel bilinear unmixing approach for reconsideration of subpixel classification of land cover, Computers and Electronics in Agriculture, Volume 152, 2018, Pages 126-140.

[9] A. Karnieli, N. Agam, R. T. Pinker et al., "Use of NDVI and land surface temperature for drought assessment: merits and limitations," Journal of Climate, vol. 23, no. 3, pp. 618–633, 2010..

[10] R. P. Sripada, R.W. Heiniger, J. G.White, and R.Weisz, "Aerial color infrared photography for determining late-season nitrogen requirements in corn," Agronomy Journal, vol. 97, no. 5, pp. 1443–1451, 2005.

[11] C. F. Jordan, "Derivation of leaf-area index from quality of light on the forest floor," Ecology, vol. 50, no. 4, pp. 663–666, 1969.

[12] A. J. Richardson and C. Weigand, "Distinguishing vegetation from soil background information," Photogrammetric Engineering and Remote Sensing, p. 43, 1977.

[13] Reference: Rouse, J., R. Haas, J. Schell, and D. Deering. Monitoring Vegetation Systems in the Great Plains with ERTS. Third ERTS Symposium, NASA (1973): 309-317.

[14] Y. J. Kaufman and D. Tanr´e, "Atmospherically Resistant Vegetation Index (ARVI) for EOS-MODIS," IEEE Transactions on Geoscience and Remote Sensing, vol. 30, no. 2, pp. 261–270, 1992.

[15] Reference: Gitelson, A., Y. Kaufman, and M. Merzylak. "Use of a Green Channel in Remote Sensing of Global Vegetation from EOS-MODIS." Remote Sensing of Environment 58 (1996): 289-298.

[16] Huete, A. "A Soil-Adjusted Vegetation Index (SAVI)." Remote Sensing of Environment 25 (1988): 295-309.

[17] Rondeaux, G., M. Steven, and F. Baret. "Optimization of Soil-Adjusted Vegetation Indices." Remote Sensing of Environment 55 (1996): 95-107.

[18] Qi, J., A. Chehbouni, A. Huete, Y. Kerr, and S. Sorooshian. "A Modified Soil Adjusted Vegetation Index." Remote Sensing of Environment 48 (1994): 119-126.

[19] Haboudane, D., et al. "Hyperspectral Vegetation Indices and Novel Algorithms for Predicting Green LAI of Crop Canopies: Modeling and Validation in the Context of Precision Agriculture." Remote Sensing of Environment 90 (2004): 337-352.

[20] Jopia, A.; Zambrano, F.; Pérez-Martínez, W.; Vidal-Páez, P.; Molina, J.; de la Hoz Mardones, F. Time-Series of Vegetation Indices (VNIR/SWIR) Derived from Sentinel-2 (A/B) to Assess Turgor Pressure in Kiwifruit. ISPRS Int. J. Geo-Inf. 2020, 9, 641. https://doi.org/10.3390/ijgi9110641

[21] Hardisky, M.A.; Klemas, V.; Smart, R.M. The Influence of Soil Salinity, Growth Form, and Leaf Moisture on the Spectral Radiance of Spartina alterniflora Canopies. Photogramm. Eng. Remote Sens. 1983, 49, 77–83. 39. Gao, B.C. NDWI—A normalized difference water index for remote sensing of vegetation liquid water from space. Remote Sens. Environ. 1996, 58, 257–266

[22] Key, C.H.; Benson, N.; Ohlen, D.; Howard, S.; McKinley, R.; Zhu, Z. The Normalized Burn Ratio and Relationships to Burn Severity. 2002. Available online: https://www.yumpu.com/en/document/view/24226870/the-normalized-burn-ratio-and-relationships-to-burn-severity- (accessed on 26 October 2020)

[23] Ceccato, P.; Flasse, S.; Grégoire, J.M. Designing a spectral index to estimate vegetation water content from remote sensing data: Part 1: Theoretical approach. Remote Sens. Environ. 2002, 82, 188–197

[24] Pinder, J.E., III; Mcleod, K.W. Indications of Relative Drought Stress in Longleaf Pine from Thematic Mapper Data. Photogramm. Eng. Remote Sens. 1999, 65, 495–501

[25] Chen, X.; Guo, Z.; Chen, J.; Yang, W.; Yao, Y.; Zhang, C.; Cui, X.; Cao, X. Replacing the Red Band with the Red-SWIR Band (0.74ρred+0.26ρswir) Can Reduce the Sensitivity of Vegetation Indices to Soil Background. *Remote Sens.* 2019, *11*, 851. https://doi.org/10.3390/rs11070851

[26] Syeda Refat Sultana, et al., Normalized Difference Vegetation Index as a Tool for Wheat Yield Estimation: A Case Study from Faisalabad, Pakistan, The Scientific World Journal, 2014.

[27] Gao, B.C. 1996. NDWI : A normalized difference water index for remote sensing of vegetation liquid water from space. Remote Sensing of Environment 58: 257-266

[28] Xu, H. "Modification of Normalised Difference Water Index (NDWI) to Enhance Open Water Features in Remotely Sensed Imagery."

This work is licensed under a Creative Commons Attribution-NonCommercial-NoDerivatives 4.0 License. For more information, see https://creativecommons.org/licenses/by-nc-nd/4.0/

This article has been accepted for publication in a future issue of this journal, but has not been fully edited. Content may change prior to final publication. Citation information: DOI 10.1109/ACCESS.2021.3124453, IEEE Access

International Journal of Remote Sensing 27, No. 14 (2006): 3025-3033." (ESRI, 2018)

[29] Jopia, A.; Zambrano, F.; Pérez-Martínez, W.; Vidal-Páez, P.; Molina, J.; de la Hoz Mardones, F. Time-Series of Vegetation Indices (VNIR/SWIR) Derived from Sentinel-2 (A/B) to Assess Turgor Pressure in Kiwifruit. ISPRS Int. J. Geo-Inf. 2020, 9, 641. https://doi.org/10.3390/ijgi9110641

[30] Andrés Viña, Anatoly A. Gitelson, Anthony L. Nguy-Robertson, Yi Peng, Comparison of different vegetation indices for the remote assessment of green leaf area index of crops, Remote Sensing of Environment, Volume 115, Issue 12, 2011, Pages 3468-3478,

[31] Available at: https://www.hyspex.com/hyspex-products/hyspex-classic/hyspex-swir-384/ (accessed on 13.05.2021)

[32] Available at: https://www.hyspex.com/hyspex-products/hyspex-classic/hyspex-vnir-1800/ (accessed on 13.05.2021)

[33] Available at: https://www.usgs.gov/centers/eros/science/usgs-eros-archive-earth-observing-one-eo-1-hyperion?qt-science_center_objects=0#qt-science_center_objects (accessed on 13.05.2021)

[34] Available at: https://www.l3harrisgeospatial.com/Software-Technology/ENVI (accessed on 14.06.2021)

[35] Huete, A., et al. "Overview of the Radiometric and Biophysical Performance of the MODIS Vegetation Indices." *Remote Sensing of Environment* 83 (2002):195–213.

[36] Available at: https://www.qgis.org/en/site/about/index.html (accessed on 05.09.2021)

[37] Jackson, T., et al. "Vegetation Water Content Mapping Using Landsat Data Derived Normalized Difference Water Index for Corn and Soybeans." *Remote Sensing of Environment* 92 (2004): 475-482.

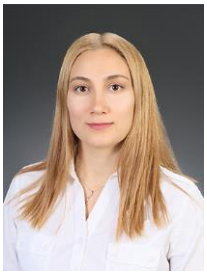
[38] Gao, B. "Normalized Difference Water Index for Remote Sensing of Vegetation Liquid Water from Space." Proceedings of SPIE 2480 (1995): 225-236.



Yucel CIMTAY graduated from Bilkent University's Electrical & Electronics Engineering department with a bachelor's degree in 2008. In 2018, he finished his PhD at Ankara University. Between 2013 to 2018, he worked as an R&D Engineer for HAVELSAN A.S. Between 2018 and 2020; he worked as a Postdoctoral Research Associate at the Institute for Digital Technologies, Loughborough University London. He is currently an Assistant Professor at TED University.



Büşra ÖZBAY received a bachelor's degree from Bilkent University, Turkey. She has been working at HAVELSAN for 7 years as an R & D Engineer. Her interests are image processing and video processing.



Gokce NUR YILMAZ received her PhD degree from the I-Lab Multimedia Communication Research Group, University of Surrey, UK, in 2011. She worked at the Electrical Electronics Engineering Department in Kirikkale University, Turkey, initially as a Research Fellow (2005), then progressing onto a Dr. Research Fellow (2011-2012), then to an Assistant Professor Dr. (2012-2018) and subsequently an Associate Professor Dr. (2018-2020). She was a Part-Time Lecturer in the University of Turkish Aeronautical Association, Turkey, between 2014 and 2015. She visited the University of Coimbra, Portuguese (2014) and Rome Tre University, Italy (2018) as a guest lecturer and researcher, respectively. She is working at TED University Computer Engineering Department, Turkey, as an Associate Professor Dr. from 2020 onwards.



Eda BOZDEMIR graduated from Uludag University Medical Faculty with MD degree in 2012. In 2016, she started her first postdoctoral fellowship at Cell Systems and Anatomy Department at University of Texas Health Science Center at San Antonio and have continued as a visiting scientist at Childrens Hospital of Philadelphia. Since 2020, she has been working as a postdoctoral research scientist at Columbia University.

This work is licensed under a Creative Commons Attribution-NonCommercial-NoDerivatives 4.0 License. For more information, see https://creativecommons.org/licenses/by-nc-nd/4.0/